Supplementary Information

Aromatic character of planar boron-based clusters revisited by ring current calculations

Hung Tan Pham,[a,b] Kie Zen Lim[c], Remco W. A. Havenith[c] and Minh Tho Nguyen[d,*]

[a] *Computational Chemistry Group, Ton Duc Thang University, Ho Chi Minh City, Vietnam*

[b] *Faculty of Applied Sciences, Ton Duc Thang University, Ho Chi Minh City, Vietnam*

[c] *Theoretical Chemistry, Zernike Institute for Advanced Materials and Stratingh Institute for Chemistry, University of Groningen, NL-9747 AG Groningen, The Netherlands Netherlands and Ghent Quantum Chemistry Group, Department of Inorganic and Physical Chemistry, Ghent University, Krijgslaan 281 (S3), B-9000 Gent, Belgium*

[d] *Department of Chemistry, KU Leuven, Celestijnenlaan 200F, B-3001 Leuven, Belgium.*

The file contains:

* Email: minh.nguyen@chem.kuleuven.be

Figure S1. The possible transitions of B_3^+ cluster.

Figure S2. The total, π and σ ring current maps of B_7^-, $B_8^{0/2-}$ and B_9^- clusters. The ring current density was calculated using B3LYP/6-311G* method.

Figure S3. Schematic orbital-energy level for the symmetry allowed virtual excitations in the B7- boron cluster. Rotationally (translationally) allowed excitation is shown as hollow (solid) arrow.

Figure S4. Schematic orbital-energy level for the symmetry allowed virtual excitations in the $B10^{2-}$ boron cluster. Rotationally (translationally) allowed excitation is shown as hollow (solid) arrow.

Figure S5. The MOs have main contributon to π and σ ring current of B_{12}.

Figure S6. Schematic orbital-energy level for the symmetry allowed virtual excitations in the $B16^{2-}$ boron cluster. Rotationally (translationally) allowed excitation is shown as hollow (solid) arrow.

Figure S7. The ring current maps of MOs which has main contribution to π and σ ring current density of B_{19}^- and B_{18}^{2-}.

Figure S8. The ring current maps of MOs which has main contribution to π and σ ring current density of a) $Li_7B_5H_5^+$ and b) $B@B_5H_5^+$

Figure S9. The ring current maps of M@B6H6q with M=Co, Fe and Mn; q=+1,0, -1.

Figure S10. The current density of MOs of $Fe@B_6H_6$

Figure S11. The ring current maps of σ MOs (a) π-MOs (b) for $Fe@B_7H_7$

Figure S12. The ring current maps of B_nC_m cluster which isolectronic with B_{10}^{2-}

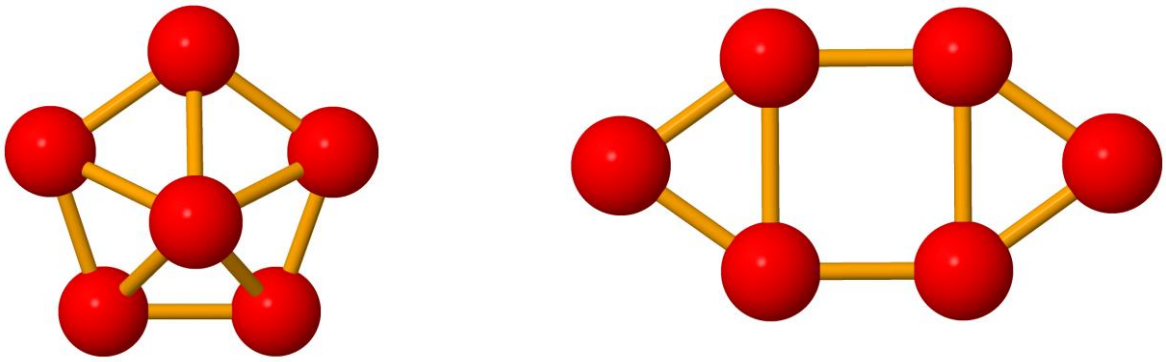

B6 (C_{5v} $^1A_1$) **B6^{2-}** (D_{2h} ^1A_g)

Scheme 1. Geometries of the most stable B_6 and B_6^{2-} clusters

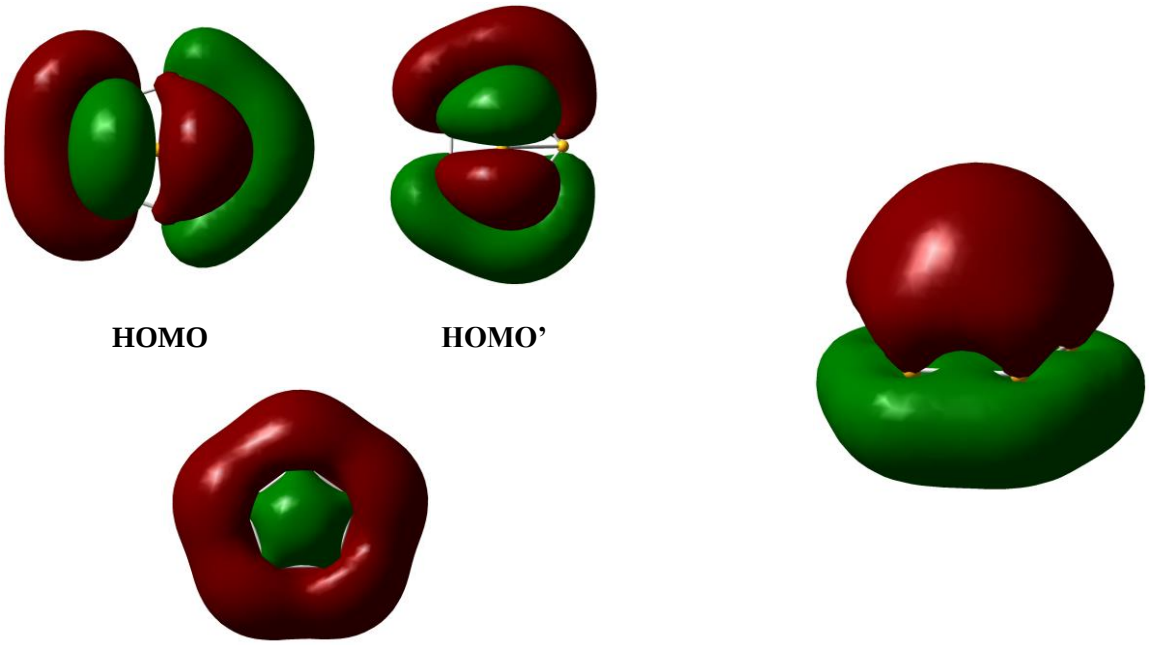

HOMO **HOMO'**

HOMO-1 **HOMO-3**

σ-MOs **π-MO**

Scheme 2. Shape of the delocalized π and σ MOs of B_6.

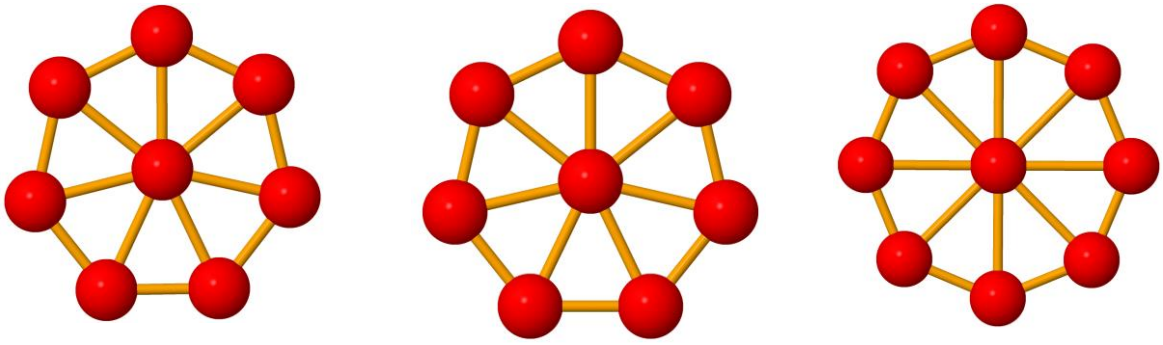

B_8 ($^3B_2$' D_{7h}) **B_8^{2-}** ($^1A_1$' D_{7h}) **B_9^-** ($^1A_{1g}$ D_{8h})

Scheme 3. Optimized geometries of the lowest-lying structures of B_8, B_8^{2-} and B_9^-.

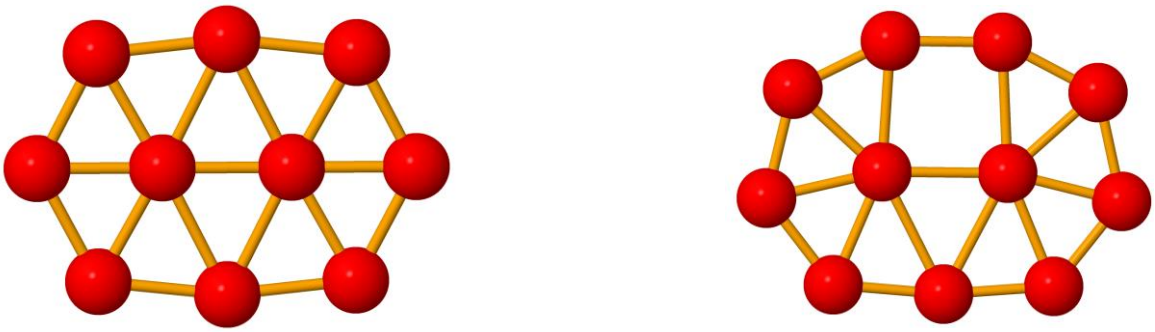

B_{10}^{2-} (C_{2v} $^1A_1$) **B_{11}^-** (C_{2v} $^1A_1$)

Scheme 4. Optimized structures of the anions B_{10}^{2-} and B_{11}^-.

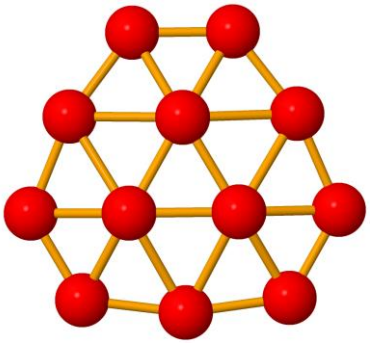

B12 (C_{3v} $^1A_1$)

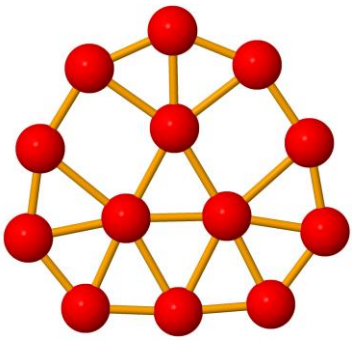

B13$^+$ (C_{3v} $^1A_1$)

Scheme 5. The optimized structure of B_{12} and B_{13}^+.

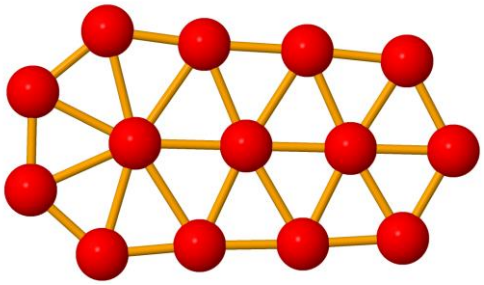

B14^{2-} (C_{2v} $^1A_1$)

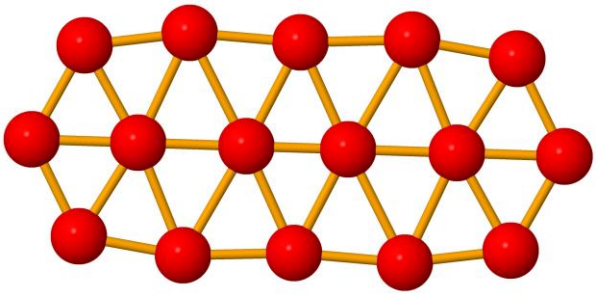

B16^{2-} (D_{2h} ^1A_g)

Scheme 6. Optimized structure of the elongated dianions B_{14}^{2-} and B_{16}^{2-}.

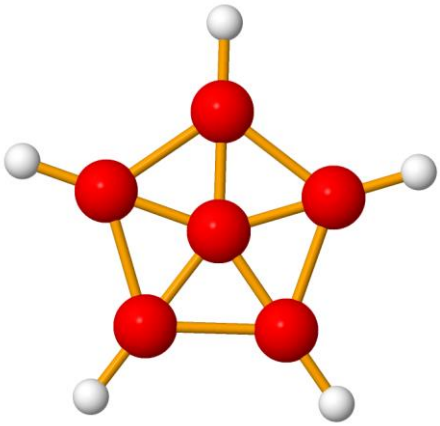

B6H5$^+$ (D_{5h} $^1A_1$')

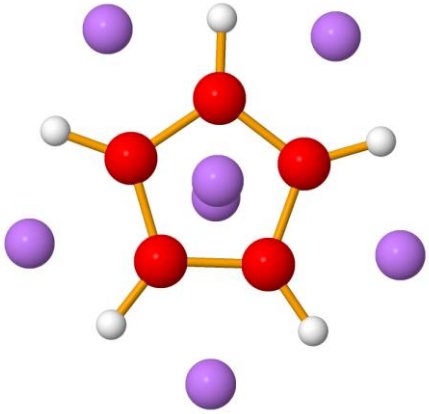

Li7B5H5$^+$ (D_{5h} $^1A_1$')

Scheme 7. Optimized structures of $B_6H_5^+$ and $Li_7B_5H_5^+$

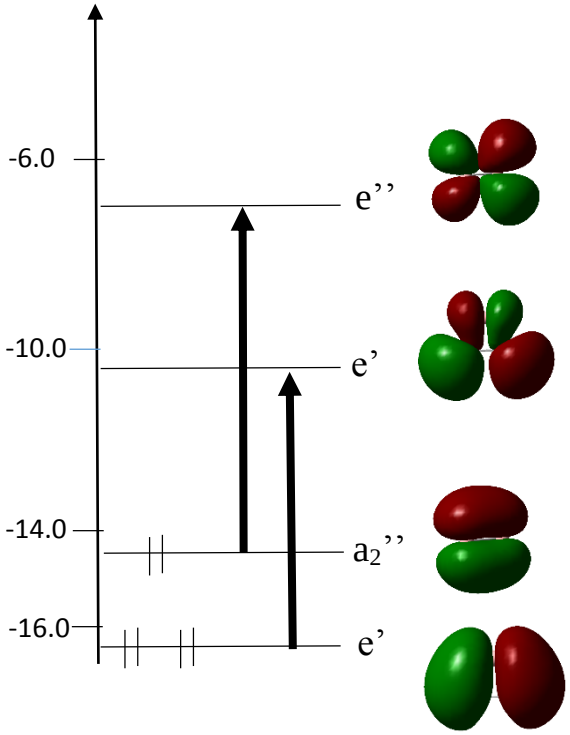

Figure S1. The possible transitions of B_3^+ cluster.

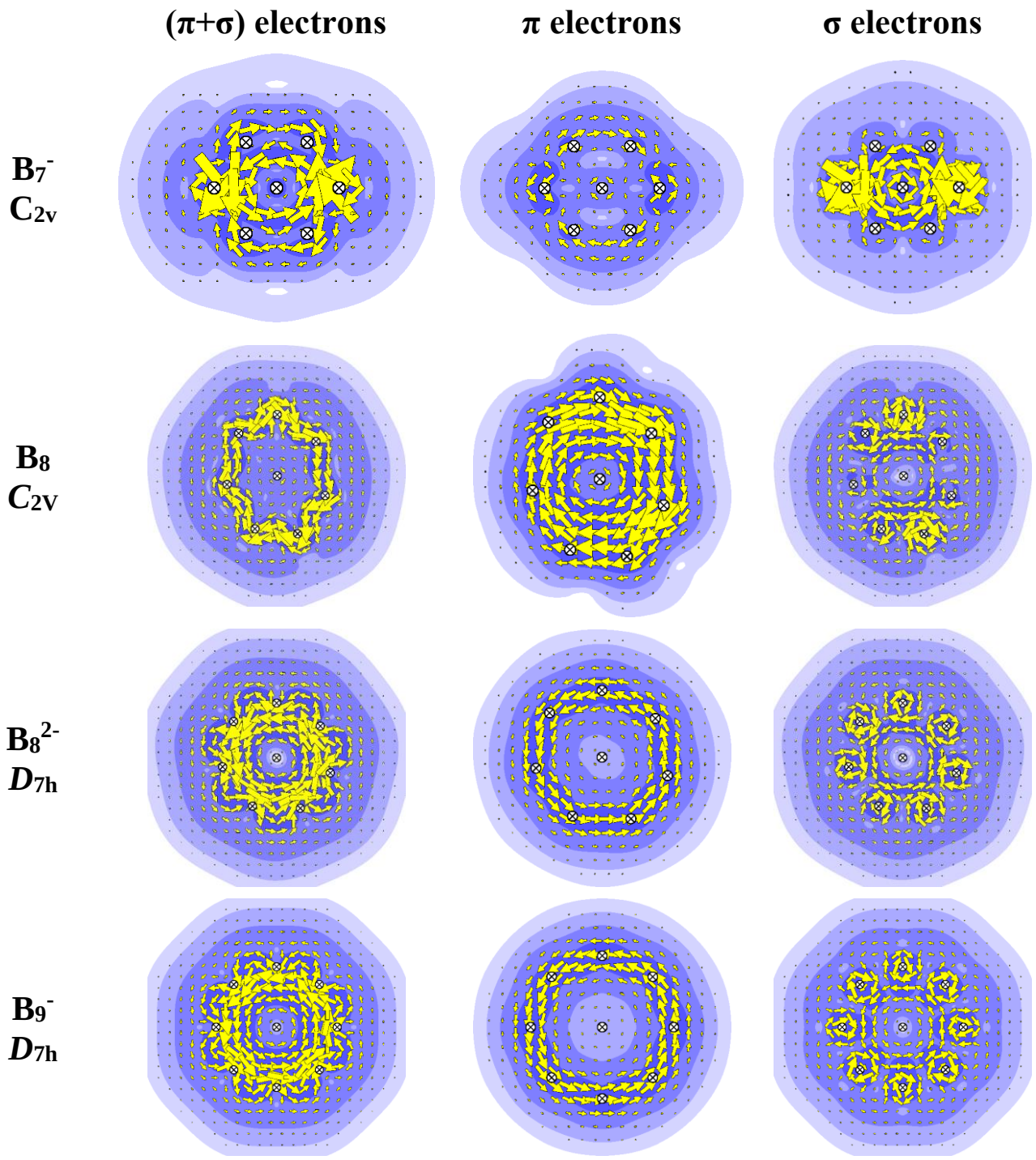

Figure S2. The total, π and σ ring current maps of B_7^-, $B_8^{0/2-}$ and B_9^- clusters. The ring current density was calculated using B3LYP/6-311G* method.

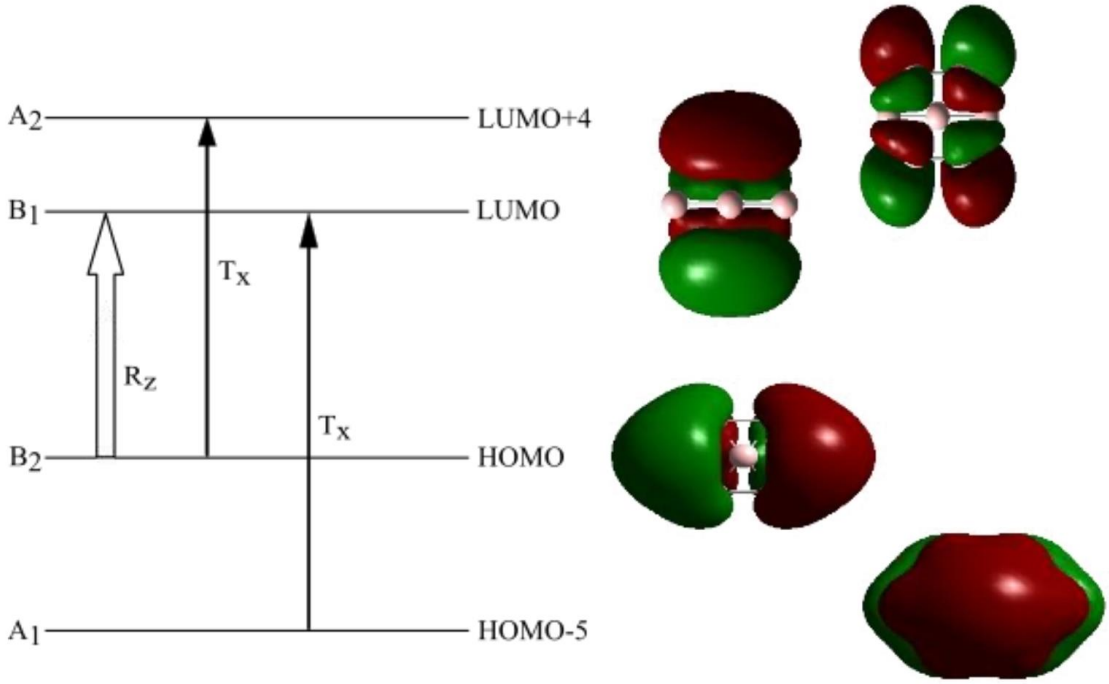

Figure S3. Schematic orbital-energy level for the symmetry allowed virtual excitations in the B_7^- boron cluster. Rotationally (translationally) allowed excitation is shown as hollow (solid) arrow.

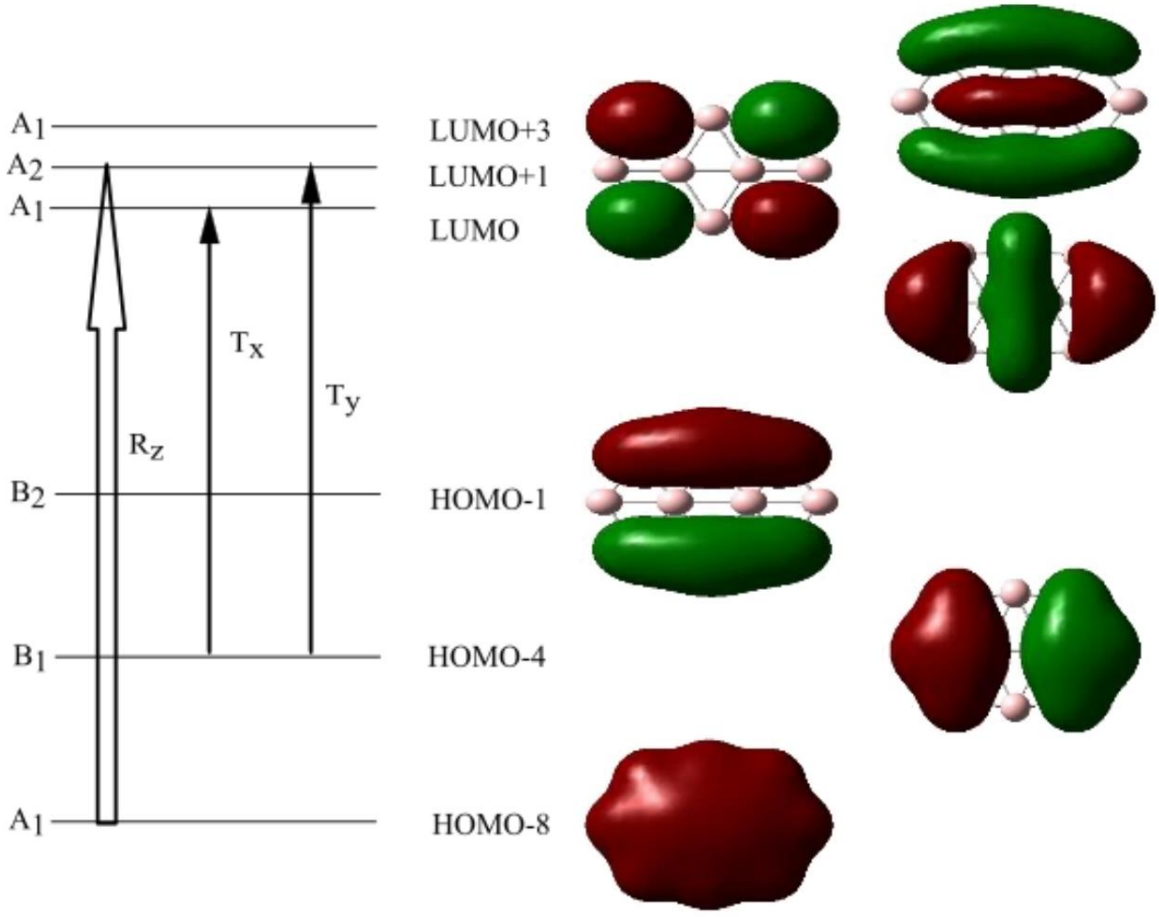

Figure S4. Schematic orbital-energy level for the symmetry allowed virtual excitations in the B_{10}^{2-} boron cluster. Rotationally (translationally) allowed excitation is shown as hollow (solid) arrow.

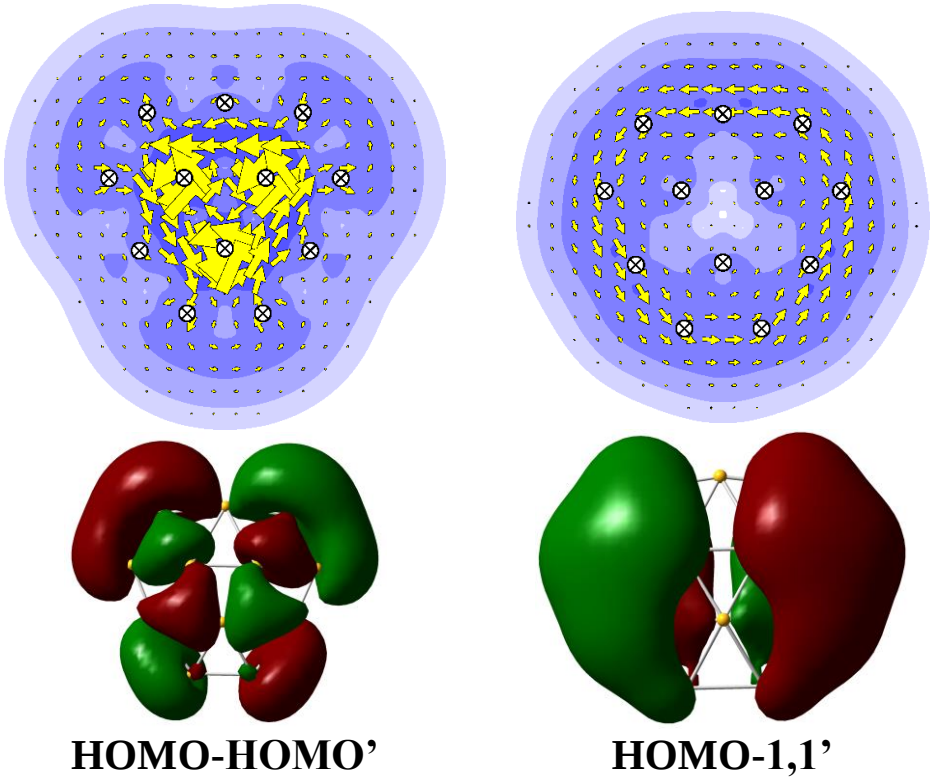

Figure S5. The MOs have main contributon to π and σ ring current of B_{12}.

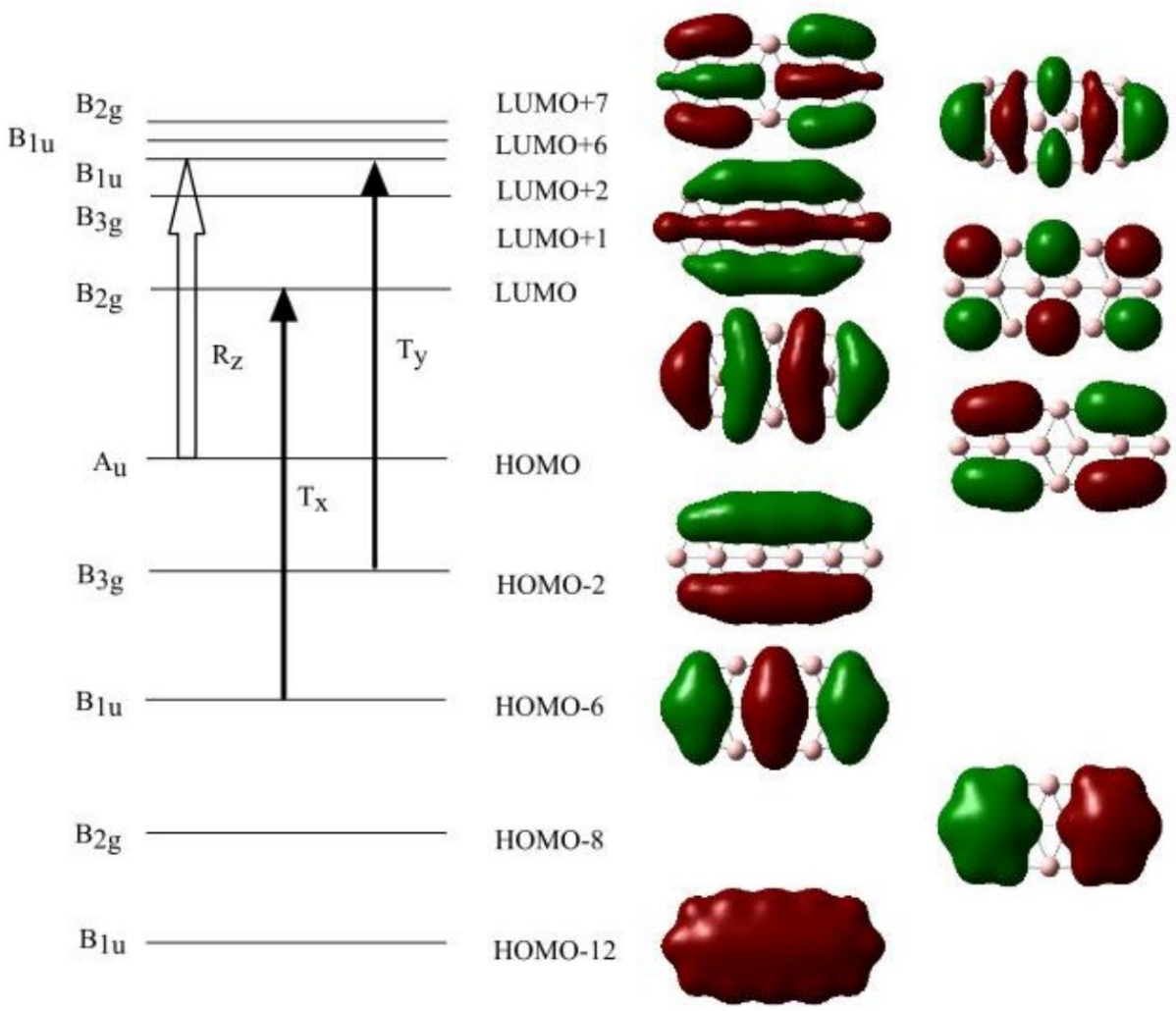

Figure S6. Schematic orbital-energy level for the symmetry allowed virtual excitations in the B_{16}^{2-} boron cluster. Rotationally (translationally) allowed excitation is shown as hollow (solid) arrow.

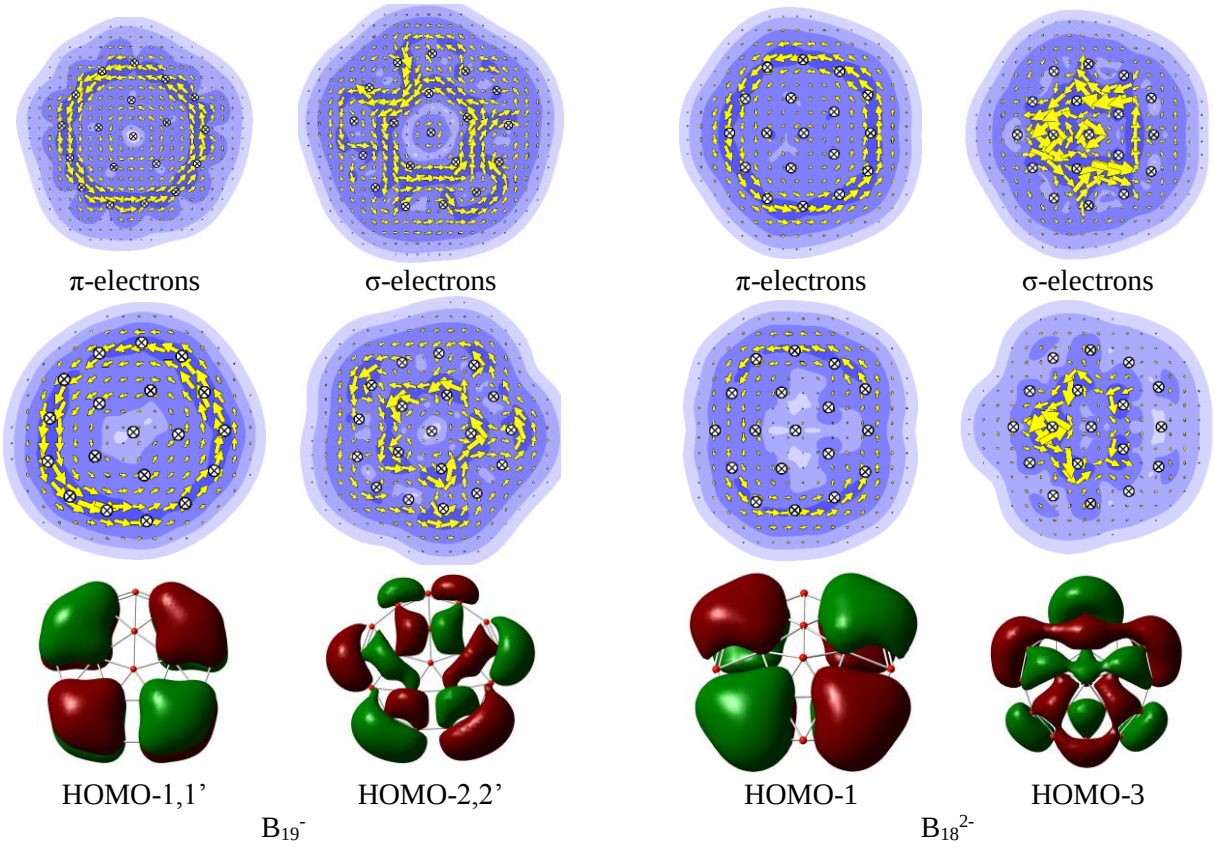

Figure S7. The ring current maps of MOs which has main contribution to π and σ ring current density of B_{19}^- and B_{18}^{2-}.

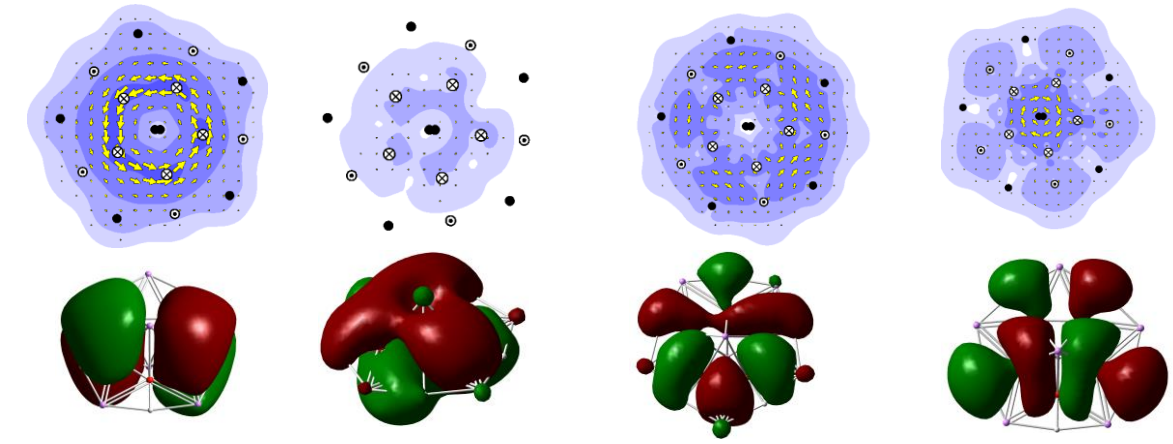

a)

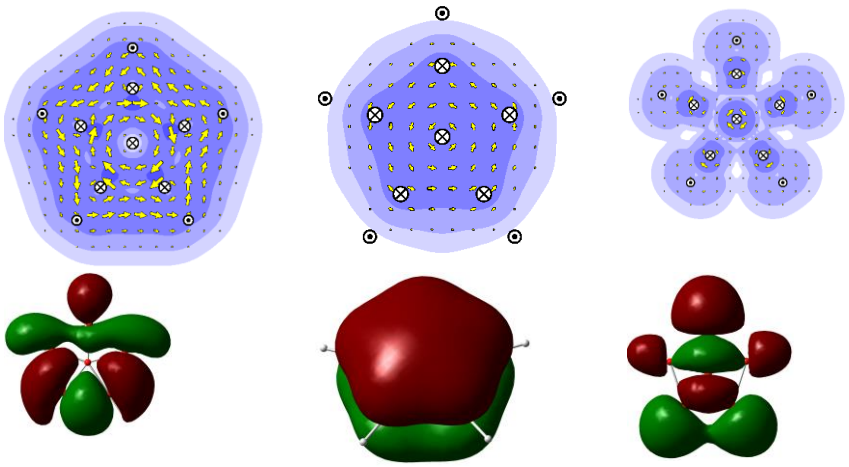

b)

Figure S8. The ring current maps of MOs which has main contribution to π and σ ring current density of a) $Li_7B_5H_5^+$ and b) $B@B_5H_5^+$

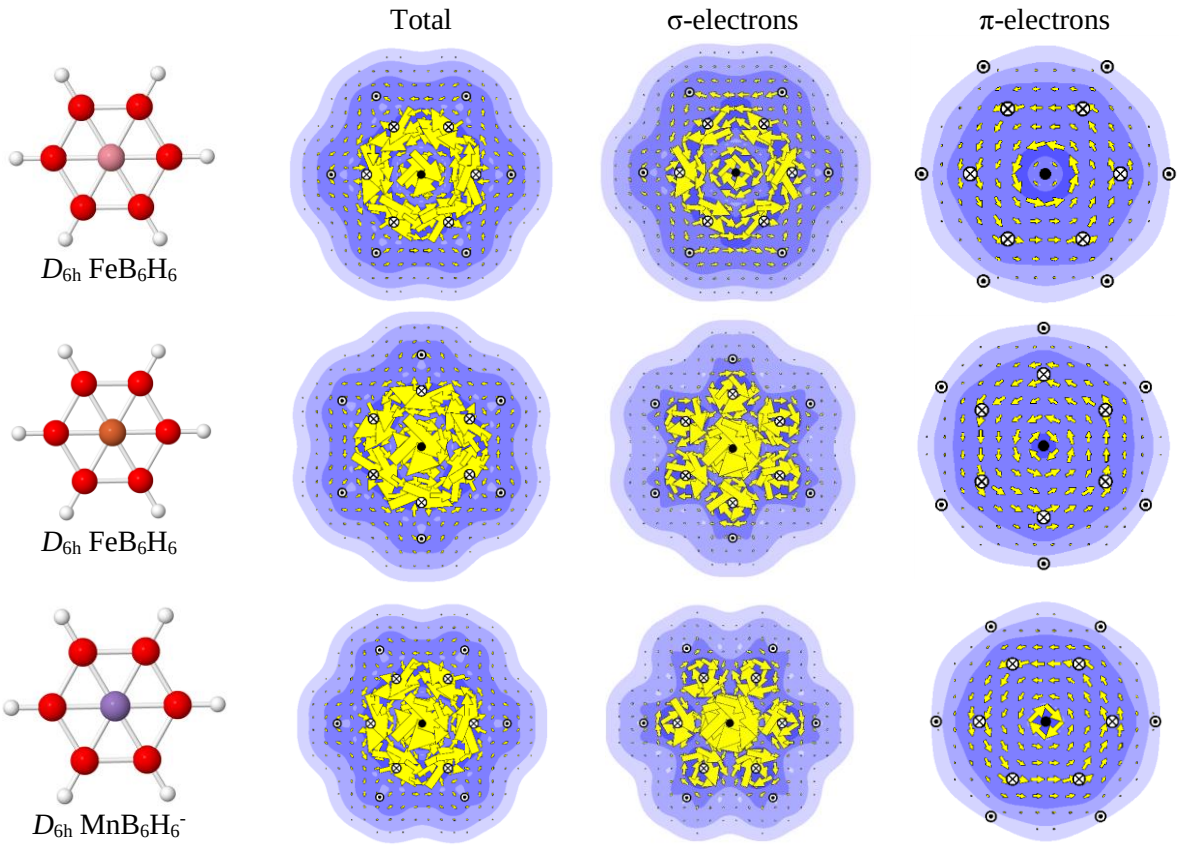

Figure S9. The ring current maps of M@B6H6q with M=Co, Fe and Mn; q=+1,0, -1.

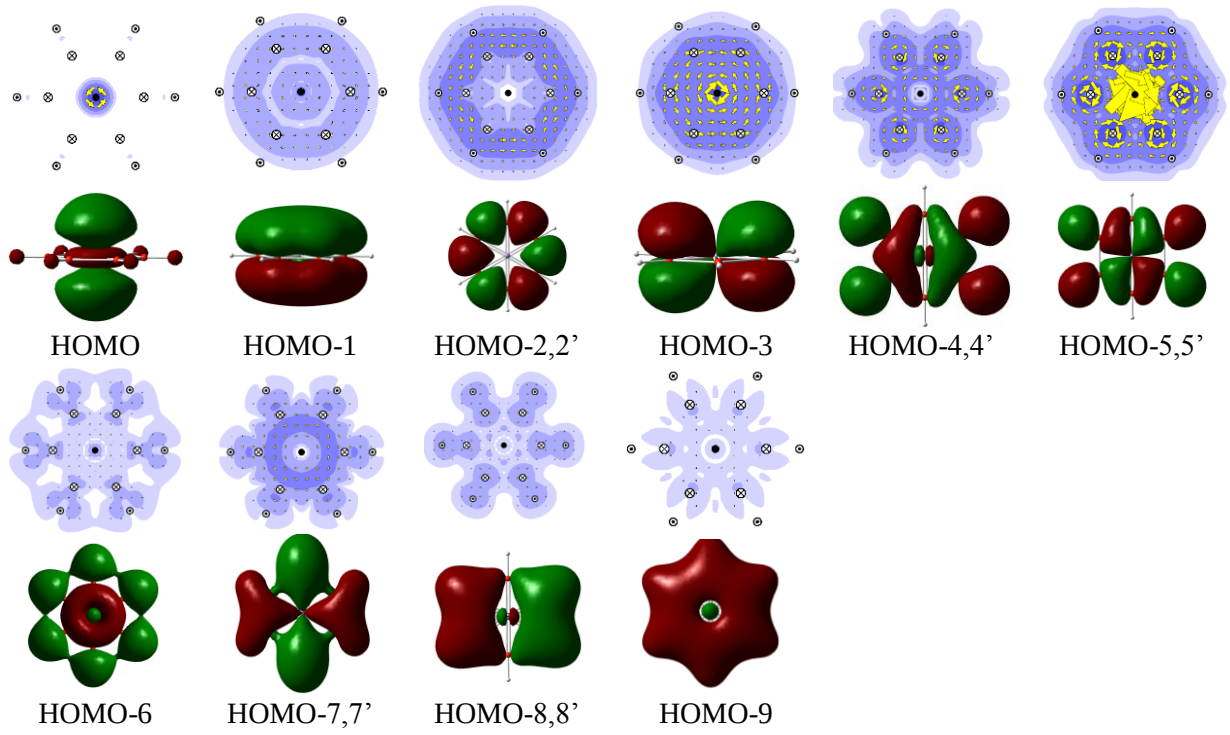

Figure S10. The current density of MOs of $Fe@B_6H_6$

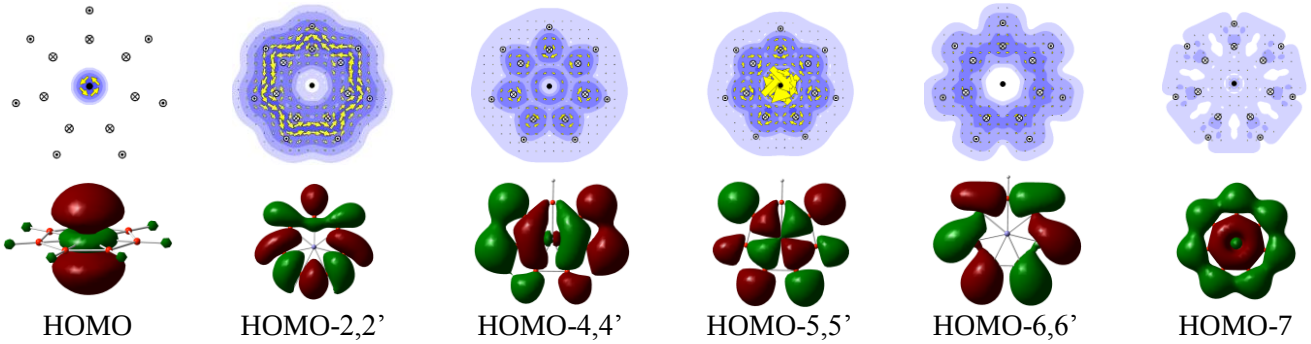

a)

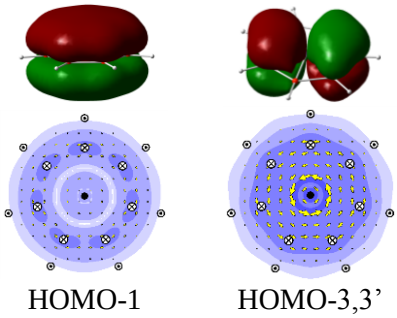

b)

Figure S11. The ring current maps of σ MOs (a) π-MOs (b) for $Fe@B_7H_7$

(σ+π) electrons **π-electrons** **σ-electrons**

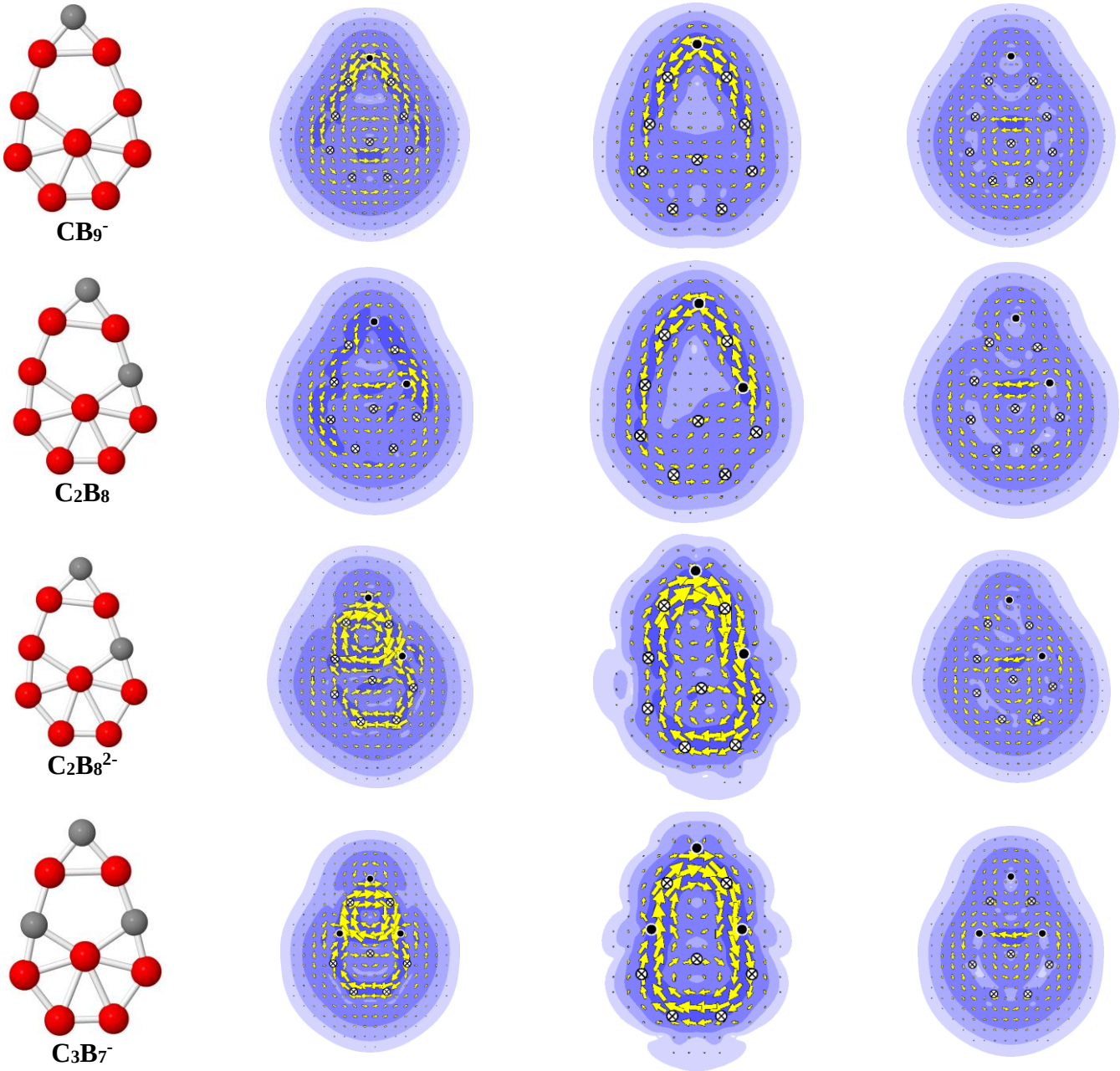

Figure S12. The ring current maps of B_nC_m cluster which isolectronic with B_{10}^{2-}